

Original Article

Intravital tumor decellularization as a new approach to cancer treatment

Zurab Kakabadze, Teona Paresishvili

Department of Clinical Anatomy, Tbilisi State Medical University, 0186 Tbilisi, Georgia

Received June 30, 2023; Accepted August 8, 2023; Epub September 15, 2023; Published September 30, 2023

Abstract: This study demonstrates the possibility of tumor decellularization in living animals. Subcutaneous Ehrlich tumor induced by isolated Ehrlich ascitic carcinoma cells in mice was used as a model. The study also presents methods for ex vivo decellularization of human gastric adenocarcinoma (HGA) and hepatocellular carcinoma (HCC) induced by diethylnitrosamine (DEN) in rat. Sodium dodecyl sulfate (SDS) and Triton X-100 were used as detergents for tumor decellularization. The detergents for HGA and HCC were administered through organ vessels. For intravital decellularization of Ehrlich's subcutaneous tumor, detergents were injected directly into the tumor parenchyma. The results of the study showed that the effectiveness of tumor decellularization using SDS and Triton X-100 depended on the size, structure, stiffness and density of the tumor, as well as on the concentration, route and speed of detergent administration. The study also showed that an hour after the initiation of decellularization, the central part of Ehrlich's tumor changed the color, and after three hours, it completely acquired a translucent white color. Chemical contamination of tissues surrounding the tumor with the detergents was not observed. Histological studies showed the complete absence of all cellular components of Ehrlich's tumor and a slightly deformed extracellular matrix (ECM). There were no loco-regional recurrences or metastases of Ehrlich's tumor within 150 days after decellularization. The developed intravital decellularization method allows the effective removal of the cellular components and the DNA content of Ehrlich's subcutaneous tumor without compromising animal health. Additionally, this method can destroy tumor ECM, which will significantly improve the delivery of anticancer drugs to the tumor cells. However, more detailed and extensive studies are needed to develop an in vivo technique for isolated decellularization of the tumor or a part of the organ with the tumor. It is also necessary to identify less toxic decellularization agents and to develop the most efficient route for their delivery to the tumor cells.

Keywords: Decellularization of organs and tissues, in vivo tumor decellularization, tumor decellularization, tumor extracellular matrix, tumor perfusion

Introduction

Throughout recent years, local drug delivery systems (LDDS) that deliver the drug directly to the tumor have attracted great interest in oncology. Compared to traditional chemotherapy, these systems avoid the systemic circulation of chemotherapy drugs, which leads to the decrease of side effects [1, 2]. At the same time, LDDSs are able to increase the intercellular concentration of antitumor drugs and provide their prolonged release, which, in turn, leads to an increase in the effectiveness of cancer treatment. However, the effectiveness of LDDS depends on many factors, including the choice of effective anticancer drugs for the treatment of a particular tumor, the chemical

and physical properties of nanomaterials used as drug carriers, their biocompatibility, structure, size and shape. The effectiveness of LDDS also depends on the ability of its components to overcome barriers created by the tumor itself, such as the dense and rigid extracellular matrix (ECM) of the tumor, its unique chaotic vasculature, and high tumor interstitial fluid pressure (TIFP) [3, 4]. In the literature, various methods of influencing these barriers are described, including the use of anti-angiogenic agents that prevent the formation of new blood vessels, vascular disrupting agents (VDA), and agents that restore altered tumor vessels [5-8]. Additionally, methods for destroying tumor ECM using collagenase [9, 10] or pegylated hyaluronidase [11, 12], methods for normalizing the

integrity of tumor vessels using antibodies against vascular endothelial growth factor (VEGF) in combination with cytotoxic therapy [1, 13, 14] are described as well. Unfortunately, all these methods cannot fully satisfy clinicians' needs. Our attention was drawn to chemotherapy methods administered through isolated organ perfusion as a new therapeutic alternative for patients with surgically unresectable tumors. For example, pancreatic cancer is the most common cause of death, and the only opportunity for a cure is surgery [15]. However, the authors point out that widespread loco-regional disease is one of the causes of unresectable cancer and that > 90% of anticancer drugs (e.g. gemcitabine) are secreted in an unchanged form, which affects toxicity but not cancer per se. To achieve higher local drug concentrations in the tumor without causing side effects, the authors used Percutaneous Isolated Pancreas Perfusion Chemotherapy [16]. Others, on the contrary, believe that isolated pancreatic perfusion should not be used as a treatment for patients with unresectable or recurrent pancreatic cancer [17]. In vivo clinical trials of isolated lung perfusion (ILuP) have been reported in four patients with unresectable metastatic lung sarcoma and four patients with diffuse bronchioloalveolar carcinoma. The treatment was conducted with doxorubicin and cisplatin via ILuP and cardiopulmonary bypass [18]. The authors note that ILuP was well tolerated by patients and it effectively delivered high doses of doxorubicin to the lungs and tumor tissues with minimal systemic toxicity. There are also reports in the literature on isolated limb perfusion (ILP) for locally advanced melanoma [19-22], isolated liver perfusion [23], intravesical chemotherapy of the bladder [24], embolization methods [25, 26] and methods of tumor ablation [27] using artery [28] and vein [29-31] catheterization techniques. However, one of the disadvantages of isolated organ perfusion is that quite frequently the efflux of anticancer drugs from the perfused organ is not complete, and results in their entry into the systemic circulation [32]. Moreover, in most protocols that are currently under development, perfusion is conducted four times per patient with at least one month between each perfusion [32]. It should also be noted that isolated organ perfusion for cancer treatment is a complex, expensive and time-consuming oper-

ation and may be associated with an increased risk of mortality.

Based on the above, we hypothesized that if isolated organ perfusion is possible, then the development of a method for in vivo isolated decellularization of the tumor could also be achievable. There are reports of the possibility of creating a bioengineered liver in vivo through decellularization and recellularization of a liver lobe in live rats [33]. It is known that the decellularization methods are effectively used in regenerative medicine to create various bioengineered organs and tissues [34-37]. Decellularization is also used for obtaining a cell-free matrix of various tumors, followed by their recellularization with tumor cells ex-vivo. Such models allow the reproduction of some features of the tumor environment, study cellular reactions, migration and proliferation of transplanted tumor cells, determine therapeutic targets of tested drugs, etc. [38-41]. An internet search for published articles on tumor decellularization in vivo was initiated using MEDLINE/PubMed (from 1990 through 2023) with keywords such as "tumor decellularization in vivo", "tumor decellularization ex vivo", "tumor decellularization", "decellularization of organs and tissues" and "methods of decellularization". Unfortunately, we did not find a single report on the possibility of tumor decellularization in vivo.

The aim of this study was to demonstrate the feasibility of intravital tumor decellularization and to provoke a discussion among readers about the advantages and possible disadvantages of this method.

Materials and methods

Animals and experimental design

The studies were carried out on 25 eight-week-old male Lewis rats and 50 outbred white laboratory male mice. The animals were purchased from the vivarium of the Tbilisi State Medical University (Tbilisi, Georgia), and kept under controlled conditions at $24 \pm 2^\circ\text{C}$ using a 12-hour day-night cycle with rodent food pellet and water ad libitum. All experiments were performed in accordance with the Guidelines for the Care and Use of Laboratory Animals. The animals use protocol was reviewed and approved by an independent ethics committee of the Tbilisi State Medical University (Georgia).

Intravital tumor decellularization

Table 1. Methods of intravital decellularization and number of animals

Group	Ehrlich subcutaneous tumor and intravital decellularization	Number of animals
1	Subcutaneous Ehrlich tumor model without treatment	10
2	Model + freezing/thawing of the tumor	10
3	Model + tumor decellularization	10
4	Model + freezing/thawing + decellularization of the tumor	10
5	Controls	10

Ehrlich subcutaneous tumor model and intravital decellularization

Isolation of tumor cells from Ehrlich's ascitic carcinoma: Ascitic fluid was aspirated by abdominal puncture to obtain tumor cells from host mice with ascitic Ehrlich carcinoma. Then, the ascitic fluid was washed with PBS (pH 7.4) and centrifuged for 10 min at 200 g. After centrifugation, part isolated tumor cells were stained with Giemsa and hematoxylin-eosin (H&E). Cell viability was determined using trypan blue in a Neubauer chamber. The animals were injected subcutaneously into the back area with 3.0 million isolated Ehrlich carcinoma cells.

Intravital decellularization of subcutaneous Ehrlich tumor

18 days after inoculation, when the tumor volume reached 200 ± 8 mm³, the animals were divided into 4 groups. Animals of the fifth group were controls. **Table 1** presents the methods of intravital decellularization and the number of animals.

All procedures were performed under prolonged anesthesia, which was achieved with a combination of medetomidine 0.3 mg/kg, midazolam 5.0 mg/kg, and butorphanol 5.0 mg/kg [45]. The preparations were diluted with sterilized saline (0.1 ml/10 g of body weight) and administered to mice intraperitoneally. To prevent hypothermia during anesthesia and after the withdrawal of animals from it, thermal support was provided using external heating devices [42].

Animals of the first group (n=10) with subcutaneous Ehrlich tumor were observed without treatment. Animals of the second group (n=10) underwent freezing/thawing of the tumor. For this procedure, two small incisions (1-1.5 cm in size) were made on the skin to the right and left

of the tumor. The tumor was frozen with a liquid nitrogen probe, which was inserted through the skin incisions. The tumor was frozen with a liquid nitrogen probe (Brymile, USA) with a method proposed by the authors [43]. The surface area of the tip of

the probe was 3 mm. The tumor freezing process was performed until the temperature at the periphery of the tumor, which was measured with thermocouples, reached -40°C. The freezing/thawing method was repeated twice. The freezing period lasted for 3 minutes. Thirty minutes after the thawing of tumor, the skin wounds were sutured.

In the animals of the third group (n=10), two small incisions were made on the skin to the right and left of the tumor, as in the animals of the second group. The tumor was perforated through skin incisions from right to left with a sharp metal rod (3.0 mm in diameter) with slow rotational movements of the fingers. After that, cannulas for intravenous injections (18 G) were inserted into both edges of the tumor, and were fixated to the surface of the tumor with cyanoacrylate (PeriAcryl-90; Multi-Use Kit; Canada). It should be noted that cyanoacrylate has hermetically sealed the space between the cannula and the tumor tissue, which prevented the penetration of detergents under the skin during the decellularization procedure. For disaggregation of tumor tissues, a warm PBS solution (37.7°C) containing 1:800 IU of collagenase A was injected through cannulas. The exposure time of collagenase A in the tumor was 20 min. Then, the tumor was washed with PBS solution for 10 minutes, and the process of decellularization was initiated. For this, 0.01%, 0.1%, and 1% sodium dodecyl sulfate (SDS; Sigma-Aldrich) in distilled water was injected using a peristaltic pump at a flow rate of 1 ml/min for three consecutive 1-hour periods each, as described by us [44]. To remove SDS, the tumor was irrigated with PBS for 10 min, and only after this step, the perfusion of the tumor was initiated with a 1% solution of Triton X-100 in water for 30 min and in saline for 10 min. After completion of intravital decellularization of the tumor, skin wounds were sutured.

Intravital tumor decellularization

Table 2. HCC model, decellularization methods and number of animals

Group	HCC and ex-vivo decellularization	Number of animals
1	HCC model without treatment	5
2	Model + freezing/thawing of the tumor	5
3	Model + tumor decellularization	5
4	Model + freezing/thawing + decellularization of the tumor	5
5	Controls	5

Animals of the fourth group (n=10) were subjected to freezing/thawing of Ehrlich's subcutaneous tumor and then proceeded to intravital decellularization as well as in animals of the third groups. Animals of the fifth group (n=10) were controls.

Model and method of HCC ex-vivo decellularization

To create HCC and develop an ex-vivo decellularization method, animals of groups 1-4 were injected intraperitoneally with 50 mg/kg diethylnitrosamine (DEN) once a week for 14 weeks, which was diluted with pure olive oil according to the method proposed by the authors [45]. Animals of the fifth group were controls. **Table 2** presents the HCC model, decellularization methods and number of animals. All animals were observed under standard vivarium conditions. The daily intake of food and water was recorded and the body weight of the animals was determined daily. Animals were sacrificed at various times after simulation (12, 18 and 24 weeks) by intraperitoneal injection of a lethal dose (100 mg/kg) of sodium pentobarbital.

At autopsy in animals of the first group (n=5) hepatectomy was performed for subsequent histopathological studies. Animals of the second group (n=5) underwent ex-vivo freezing/thawing of the liver. Animals of the third group (n=5) for ex-vivo liver decellularization, venous catheters (G 24) were inserted into the inferior vena cava (IVC) and portal vein, and the superior vena cava (SVC) was occluded. The liver was perfused through the portal vein with saline containing one unit of heparin per ml. A warm PBS solution (37.7°C) containing 1:800 IU of collagenase A was then injected to disaggregate the tumor tissues. The exposure time of collagenase A in the liver was 30 min. Next,

the liver was washed with PBS for 10 minutes and the process of decellularization was started. To do this, 0.01%, 0.1%, and 1% SDS in distilled water was injected through the portal vein using a peristaltic pump at a flow rate of 1 ml/min for three consecutive 8-hour periods each.

To remove SDS, the liver was washed with PBS for 20 min, 1% Triton X-100 in water for 1 h, and saline for 20 min. The outflow of detergents was carried out through a catheter inserted into the inferior vena cava. After ex-vivo decellularization of HCC, a hepatectomy was performed for subsequent histopathological studies. In animals of the fourth group (n=5) at autopsy, the liver was subjected to freezing/thawing as described above, and then ex-vivo decellularization was performed.

Ex-vivo human gastric adenocarcinoma decellularization method

Gastric adenocarcinoma was obtained after signing an informed consent from a 65-year-old patient after gastrectomy. Immediately after gastrectomy, the stomach was transferred to the laboratory and washed in saline for 10 minutes. Next, polyethylene catheters were introduced into the arteries and veins of the stomach, and were fixated to the walls of the vessels. Heparin-containing saline solution was injected through arterial catheters to wash out the blood. After completing the perfusion, the stomach was placed in a freezer for 12 hours at a temperature of -80°C. Afterwards, the stomach was thawed, and a warm PBS solution (37.7°C) containing 1:800 IU of collagenase A (Sigma-Aldrich) was injected through the arterial catheters. The exposure time of collagenase A in the tumor was 30 min. Then, the stomach was washed with PBS solution for 10 minutes, and the process of decellularization was initiated. For this, 0.01%, 0.1%, and 1% SDS in distilled water was injected into the arteries of the stomach using a peristaltic pump at a flow rate of 1 ml/min for three consecutive 4-hour periods each. The stomach was irrigated with PBS for 30 min, and only after this step, the perfusion of the stomach was initiated with a 1% solution of Triton X-100 in water for 1 hours and

Intravital tumor decellularization

in saline for 30 min. The outflow of detergents was carried out through a catheter inserted into the veins of the stomach.

Postoperative care

All animals were maintained under standard laboratory conditions on normal day and night cycles with ad libitum rodent food pellets and water. On days 7, 14, 30, 60, 90, and 150, the animals were euthanized using a combination of intraperitoneal administration of ketamine and xylazine, followed by laparotomy, aortic rupture, and exsanguination.

Tumor volume determination

The tumor volume was measured at autopsy after sampling for histopathological analysis at various time points. Tumor volume was calculated using the formula: volume = length × width × height × ($\pi/6$).

Tumor tissue DNA measurement

DNA was isolated from 30 mg tissue samples before and after decellularization of tumor with a commercial kit (G-spin Total DNA Extraction Mini kit; iNtRON Biotechnology, Inc., Seongnam, South Korea). Total DNA content was measured by spectrophotometer at 260 nm (NanoDrop 1000; Thermo Fisher Scientific, Inc., Waltham, MA, USA).

Measurement of tumor tissue density

Measurement of tissue density before and at various times after decellularization of human gastric adenocarcinoma, DEN-induced hepatocellular carcinoma in rats, and subcutaneous Ehrlich tumor was performed by biopsy using a 1 mm glass tube. The height of the tumor tissue column in the tube was measured and, on its basis, the tumor volume was calculated using the cylinder volume formula: $V = \pi r^2 h$, where V is the volume of the obtained tumor tissue; r is the tube inner radius; h is the height of the tumor tissue column inside the tube. After that, the contents of the tube were weighed and the tumor tissue density was determined by the formula $\rho = m/V$, where ρ is the tissue density; m is the mass of the removed tumor tissue.

Assessment of macroscopic decellularization

Macroscopic decellularization was also assessed according to the method proposed by

the authors [46]. This method is based on two interrelated criteria: the distribution and extent of tumor tissue remnants and the distribution and extent of translucent areas.

Histopathological examination

For the histopathological examination, the Ehrlich tumor and its surrounding tissues were fixed in 10% neutral buffered formalin for 24 hours at a room temperature and were embedded in paraffin. Tissue sections of 5- μ m thickness were stained with H&E, 4', 6-diamidino-2-phenylindole (DAPI) and Masson's trichrome according to the manufacturers' protocols. Immunostaining with anti-Ki67 (incubation time, 20 min; clone MM1; dilution 1:200; cat. no. PA0118; Leica Biosystems Newcastle Ltd.), and BSL-2 (incubation time, 20 min; Clone bcl-2/100/D5; dilution 1:100 for 30 minutes at 25°C; Leica Biosystems Newcastle Ltd.) antibodies was performed with the manual staining method using the Novolink DAB Polymer Detection system (incubation time, 20 min; cat. no. RE7260-CE; Leica Biosystems Newcastle Ltd.) in accordance with the manufacturer's recommendations. Endogenous peroxidase activity was neutralized using the Peroxidase Block reagent (3-4% (v/v) hydrogen peroxide; Novolink DAB Polymer Detection system; cat. no. RE7260-CE; Leica Biosystems Newcastle Ltd.). To reduce non-specific binding of primary antibody Novocastra Protein Block reagent was used (0.4% casein in phosphate-buffered saline, with stabilizers, surfactant and 0.2% Bronidox L as a preservative; Novolink DAB Polymer Detection system). As the secondary antibody, rabbit anti-mouse IgG (< 10 μ g/ml) in 10% (v/v) animal serum in Tris-buffered saline/0.1% ProClin™ 950 was used (Novolink DAB Polymer Detection system). All reactions for immunohistochemistry were performed at room temperature. Images were acquired using a Leica DMLB microscope (Leica Application Suite v.3.6.0, Wetzlar, Germany).

Scanning electron microscopy

The collected tumors tissues were immersed in a fixative solution containing 2.5% glutaraldehyde and 4% paraformaldehyde in 0.1 M phosphate buffer. After fixation, the samples were dehydrated in ethanol of various concentrations. The samples were then immersed in a mixture of 95% ethanol and isoamyl acetate (1:1) for 10 minutes and in pure isoamyl ace-

Intravital tumor decellularization

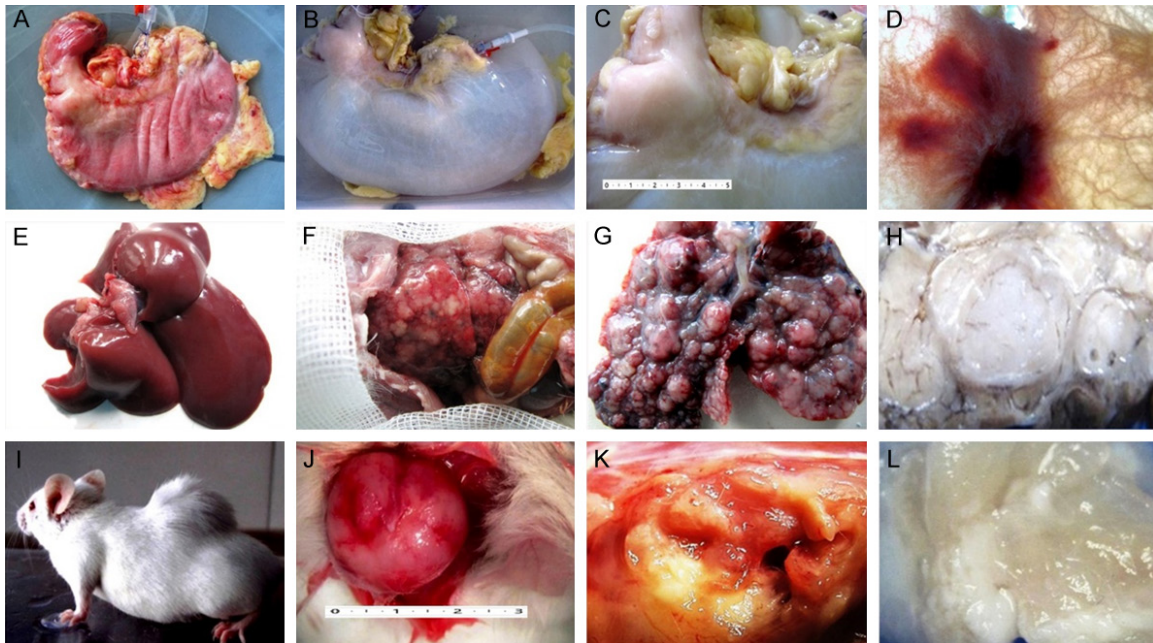


Figure 1. Various tumors before and after decellularization. A. Gross image of human gastric adenocarcinoma after gastrectomy. B. Decellularization of a whole stomach. C. Gross image of decellularization of gastric adenocarcinoma (3×4 cm). D. Stained liquid latex was injected into the gastric vessels to visualize the tumor vasculature. E. Normal liver of the rat. F. Laparotomy. HCC of the rat liver is determined. G. Gross image of DEN-induced HCC in rat. H. Rat HCC after decellularization. I. Subcutaneous Ehrlich tumor in mic. J. Gross image of subcutaneous Ehrlich tumor after skin dissection (2×2 cm). K. Sagittal section of Ehrlich's tumor. L. Decellularization process of subcutaneous Ehrlich tumor.

tate for 15 minutes. After removing the isoamyl acetate, the samples were dried using a Tousimis Samdri-780 critical point dryer (Tousimis Research Corporation). The tissues were then lightly coated with gold sputtering and visualized with a JEOL JSM-65 10 LW scanning electron microscope (JEOL, Ltd.).

Statistical analysis

Data are presented as mean ± standard error of the mean. For paired comparisons, non-parametric data or ploidy distributions, t-test, Mann-Whitney test, and Wilcoxon rank-sum test, respectively, were used using GraphPad Prism7 (GraphPad Software Inc., La Jolla, CA) and $P < 0.05$ was considered significant.

Results

The study showed that the effectiveness of tumor decellularization using SDS and Triton X-100 depended on the size, structure, stiffness and density of the tumor, as well as on the concentration, route and speed of detergent administration. For example, HCC represented

nodes that were separated from each other by a dense and rigid connective tissue capsule (**Figure 1**). This structure of the tumor significantly complicates the process of washing out cancer cells and, accordingly, requires a longer exposure to decellularizing agents, in contrast to gastric adenocarcinoma or subcutaneous Ehrlich tumor. In the process of decellularization, the liver gradually changed color and by the end of the decellularization, it became a whitish-translucent color. Examination under a light microscope of decellularized HCC showed incomplete removal of liver cells with preservation of the ECM. However, the capsule of the dysplastic nodules was deformed and contained hollow spaces in which unwashed single tumor cells were found with few remaining cell nuclei (**Figure 2**). DNA concentrations in the liver of animals with the HCC model after decellularization were 31.24 ± 2.14 ng/μl. Decellularization of human gastric adenocarcinoma using SDS and Triton X-100 demonstrated complete absence of cancer cells with slight deformation of the tumor extracellular matrix (not shown).

Intravital tumor decellularization

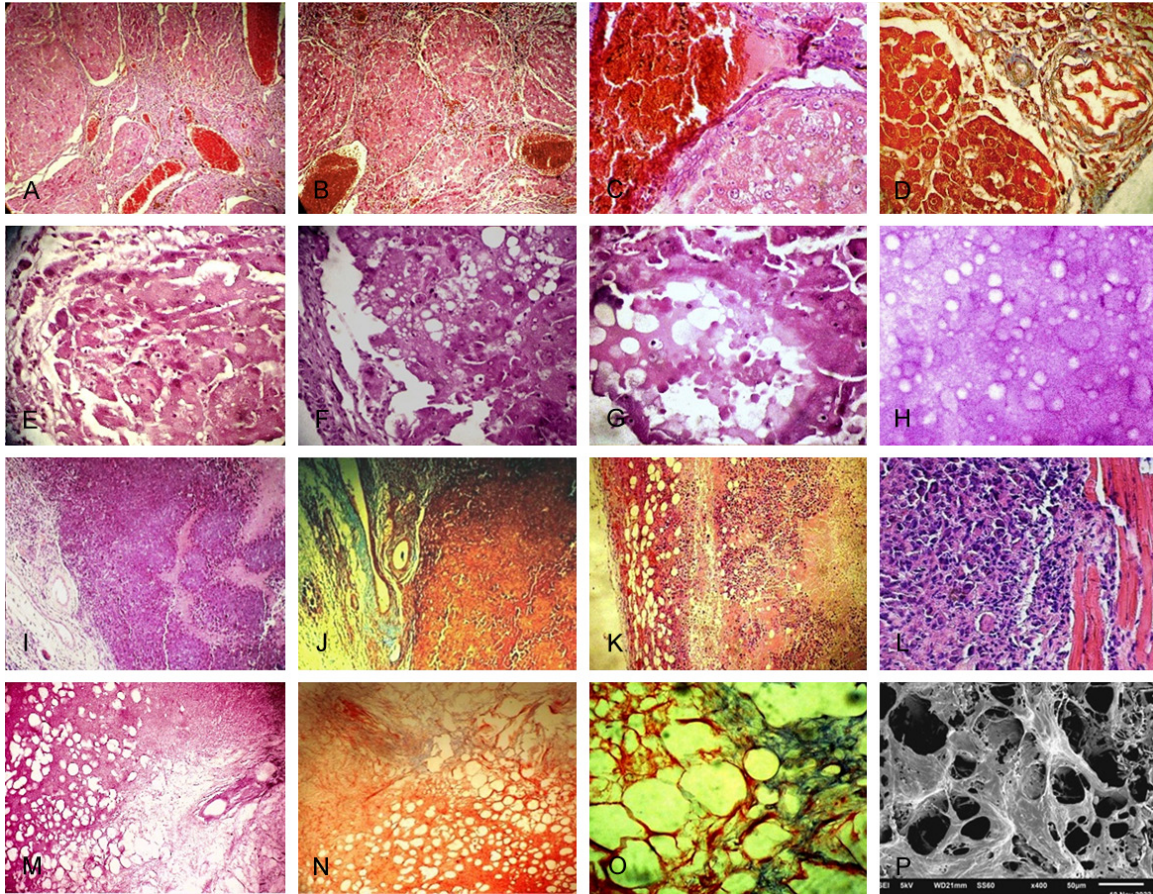


Figure 2. Gross images and histopathological picture of the tumors before and after the decellularization. A, B. Histological image of HCC. Nodes separated from each other, covered with a dense and rigid connective tissue capsule. Hematoxylin-eosin staining, $\times 200$. C. Cells with signs of HCC are clearly defined. Hematoxylin-eosin staining, $\times 400$. D. Structure of the capsule of HCC nodes. Masson's Trichrome Staining, $\times 400$. E, F. Histological picture of HCC after decellularization. HCC washing for 8 hours. G, H. Decellularization of HCC after 24 hours. Dysplastic HCC nodules are deformed and contain hollow spaces in which unwashed single tumor cells are defined with few remaining cell nuclei. Hematoxylin-eosin staining, $\times 400$. I, J. Structural heterogeneity of Ehrlich's tumor tissue, presence of areas of necrosis and inflammatory cells. Hematoxylin-eosin and Masson's trichrome staining, $\times 200$. K. Connective tissue capsule of Ehrlich's tumor with clear contours. Hematoxylin-eosin staining, $\times 400$. L. Invasion of tumor cells into muscle fibers. Hematoxylin-eosin staining, $\times 400$. M, N. Ehrlich tumor extracellular matrix 1 month after decellularization. Complete absence of tumor cells; Staining with hematoxylin-eosin and trichrome according to Masson, $\times 200$. O. The structure of the extracellular matrix of Ehrlich's tumor 2 months after decellularization. Masson trichrome coloring $\times 800$. P. Scanning electron microscopy, structure of the tumor extracellular matrix without cells.

In our study, 20 days after inoculation of isolated Ehrlich carcinoma cells, a solid oval tumor with a volume of $200 \pm 8 \text{ mm}^3$ was found under the skin in all animals. The color of the coat and skin around the tumor did not change. A study under a light microscope of sections of Ehrlich's tumor and surrounding tissues stained with hematoxylin-eosin revealed structural heterogeneity of the tumor tissue, the presence of areas of necrosis and inflammatory cells. Accumulation of tumor cells was observed both in the central and peripheral parts of the tumor, which were represented by both anaplastic and

differentiated cells. Ehrlich's tumor was completely covered with a connective tissue capsule with clear contours. Invasion of tumor cells into the surrounding tissues and the abdominal cavity was also observed. Scanning electron microscopy of the tumor showed hard and dense tissue with a large number of randomly arranged tumor cells. Due to the progression and invasion of the tumor into the surrounding tissues, all animals of this group have died within two months after modeling. In animals of the second group, after the freezing/thawing procedure, histopathological examination

of the tumor tissue showed that the arrangement of cells in the tumor parenchyma did not change. Cell morphology was homogeneous. In most tumor cells, the nuclei were broken into small clumps. Within 1.5-2 months after freezing/thawing of the tumor, 78% of the animals died from the progression and invasion of the tumor into the surrounding tissues. In animals of the third group, an hour after the start of decellularization, the central part of the tumor began to change color and after three hours it completely acquired a translucent white color. Cytological examination of the perfusate flowing from the tumor showed the presence of Ehrlich tumor cells. There was no leakage of detergents from the surface of the tumor into the surrounding tissues, which was due to reliable sealing of the cannulas with cyanoacrylate. In animals of the fourth group, after freezing/thawing and the beginning of decellularization, the liver completely acquired a translucent white color within two hours. Staining of decellularized tissues of Ehrlich's tumor with hematoxylin-eosin and Masson's trichrome in animals of the third and fourth groups, five hours after decellularization, showed the absence of all cellular components of the tumor. The DNA concentration was less than 2%. At the same time, the ECM of a decellularized tumor was a reticulate fibrous structure with unevenly distributed holes (**Figure 3**). DAPI staining of the tumor tissue showed a significant decrease in the number of tumor cell nuclei one hour after the onset of decellularization. Approximately 3 hours after decellularization, no luminescence of tumor cell nuclei was detected. Histological studies also showed that on days 5-8, a limited infiltrate consisting of polymorphonuclear leukocytes, lymphocytes and macrophages can be traced along the edges of the decellularized tumor, which may indicate a limited specific inflammatory response. Animals of the third group had small islands in the center of the tumor, consisting of necrotic tumor cells, which were surrounded by leukocytes, lymphocytes, and macrophages. In animals of the fourth group, a month after decellularization, a dense fibrous tissue with newly formed blood vessels formed around the acellular ECM of the tumor. Two months later, macrophage-like and multinucleated giant cells were found in the decellularized tissue of Ehrlich's tumor. At the same time, the ECM of the tumor was completely fragmented. Fibrous

collagen tissue was located between the fibers. Three months later, fibrous tissue was determined at the site of the decellularized ECM of Ehrlich's tumor, and the matrix itself was resorbed. Loco-regional recurrence or tumor metastases in animals of the third and fourth groups were not observed during the entire observation period. Thus, the conducted studies have shown that a protocol based on the freeze/thaw method, followed by *in vivo* tumor decellularization with SDS and Triton X-100, allows efficient removal of cellular components and DNA content. Staining with DAPI, H&E, and Masson trichrome confirmed the effective removal of most of the tumor cells.

Discussion

Ehrlich's tumor, also known as Ehrlich's ascitic carcinoma (EAC), is widely used as a model for cancer research in laboratory animals [47-49]. The development of Ehrlich's tumor in mice begins immediately after the introduction of tumor cells. These cells are usually obtained from the original Ehrlich ascites carcinoma in a donor mice and then expanded in culture to create a suspension of tumor cells. Then the tumor cells are injected either into the abdominal cavity or under the skin of experimental animals by injection. After injection, tumor cells begin to grow and form tumor masses with spread to surrounding tissues. The formed Ehrlich tumor consists of cancer cells that are usually round or irregular in shape. These tumor cells exhibit pleomorphism, which means they vary in size and shape, which is commonly seen in malignant tumors. Cells may have large nuclei and prominent nucleoli [50]. Histological analysis often shows a large number of mitotic figures, indicating active division and proliferation of tumor cells. This feature is a hallmark of fast-growing and aggressive tumors. It should be noted that Ehrlich's tumor is known for its aggressive growth and high malignancy. This model is widely used in cancer research because it shares similarities with some aspects of human cancer.

The development of subcutaneous Ehrlich tumor in mice can be conditionally divided into several stages, which may vary depending on the number of tumor cells injected and the individual immune response of the mice. In the first stage, or lag phase, isolated live Ehrlich carci-

Intravital tumor decellularization

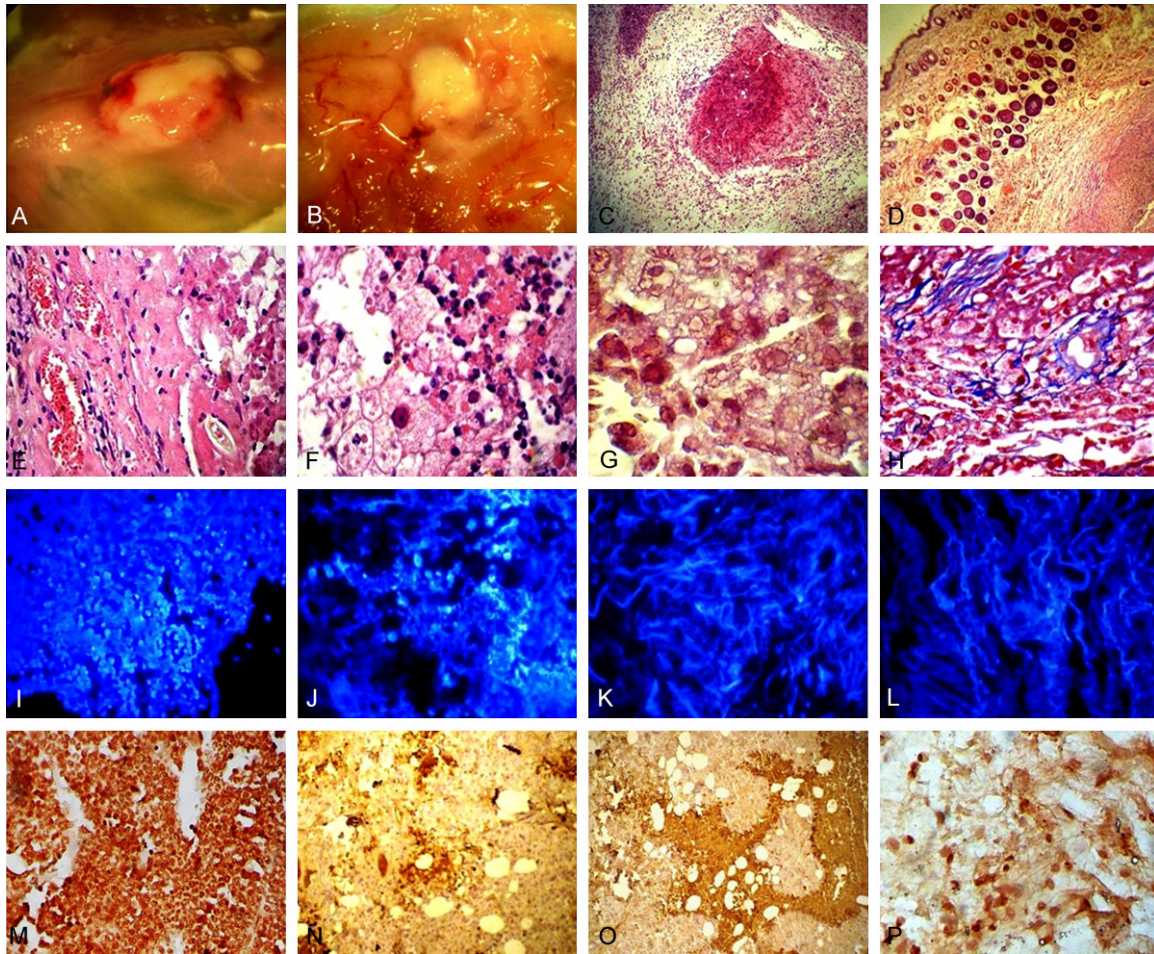


Figure 3. Gross images and histopathological picture of the Ehrlich tumor. A, B. Process of resorption of decellularized ECM Ehrlich tumor. Observation period of 30 days. C, D. Fibrous tissue is around the decellularized extracellular matrix. Hematoxylin-eosin staining, $\times 200$. E-G. There are small islands of necrotic tumor cells at various sites of the tumor, surrounded by leukocytes, lymphocytes, and macrophages. Macrophage-like and multinucleated giant cells were found. Hematoxylin-eosin staining, $\times 800$. H. Collagen fibers between necrotic tumor cells. One month after decellularization. Masson's trichrome staining, $\times 800$. I, J. One hour after decellularization. DAPI staining of tumor tissue fragments have shown a significant decrease in the number of tumor cell nuclei. K, L. 5 hours after decellularization, no luminescence of tumor cell nuclei was detected. M. Increased expression of Ki-67. Before decellularization. N. Low expression of Ki-67. One month after decellularization. O. Increased expression of Bcl-2. Before decellularization. P. Low expression of Bcl-2. One month after decellularization.

noma cells inoculated into the subcutaneous tissue adapt to the new environment, and the mice's immune system reacts to the foreign cells. At this stage, tumor cells may not show significant growth, and the immune system tries to recognize and eliminate them. In the second stage, when tumor cells overcome the immune response and adapt to the subcutaneous environment, they enter the exponential growth phase. Tumor cells rapidly divide and multiply, resulting in the formation of a palpable tumor mass under the skin. The third stage characterized by angiogenesis and vasculariza-

tion. As the tumor grows, it needs more nutrients and oxygen. The formed subcutaneous tumor secretes factors that stimulate the growth of new blood vessels from surrounding tissues, providing its blood supply. This process supports the further spread of the tumor. In the fourth stage, the tumor continues to grow and it may invade nearby tissues and structures, including muscle and connective tissue. In some cases, the tumor can even metastasize to distant organs [51-54]. However, it should be noted that Ehrlich's tumor in mice is not a direct reflection of human cancer. Therefore, the

Intravital tumor decellularization



Figure 4. Different organs and tissues before and after decellularization. A, B. Pig spleen. C, D. Pig intestine loops. E, F. Human placenta. G, H. Pig kidney. I-M. Bovine placenta and placental vessels. N, O. Bull bone. P-S. Begonia plant.

results of studies of Ehrlich tumors must be carefully extrapolated and confirmed by clinical trials in humans. However, the Ehrlich tumor in mice can be used to study various aspects of cancer, such as tumor biology, metastasis, and the development of new cancer therapies.

To develop a method for intravital decellularization of Ehrlich's subcutaneous tumor in mice, it was initially necessary to solve a number of problems: 1) Determine the detergents capable of completely removing cancer cells from a tumor in a short period. 2) Determine the most optimal ways to deliver detergents to the tumor. 3) Prevent chemical damage to the tissues surrounding the tumor and minimize the percentage of detergents entering the systemic circula-

tion. 4) Develop a protocol that maximally limits the time of tumor decellularization in-vivo.

It should be noted that for several years we have developed various protocols for the decellularization of such organs and tissues as the kidneys, spleen, intestines, lungs, human placenta, amniotic membrane, bovine placenta, umbilical cord vessels, bone, etc. (Figure 4) [42, 55-58]. Studies have shown that the combination of SDS and Triton X-100 most effectively removed all the cellular elements of organs and tissues without damaging their extracellular matrix.

Depending on the purpose of the study, various biological, chemical and mechanical methods

Intravital tumor decellularization

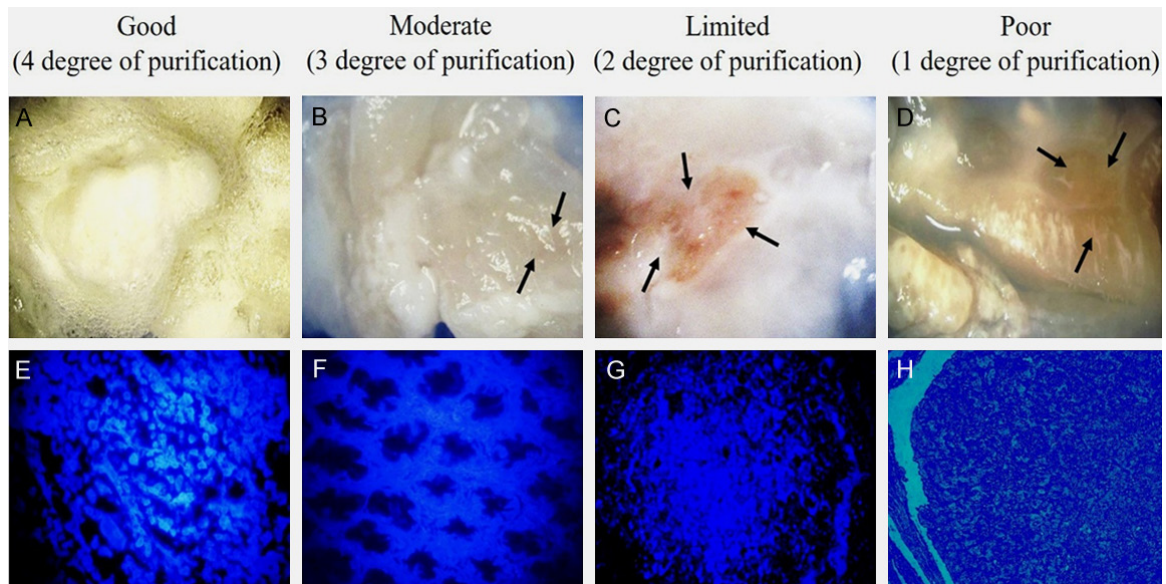


Figure 5. Results of decellularization of subcutaneous Ehrlich tumor depending on time. A. 5 hours; B. 3 hours; C. 2 hours; D. 1 hour. DAPI staining of subcutaneous Ehrlich tumor and DEN-induced hepatocellular carcinoma before and after decellularization. E. Presence of cellular nuclear material (DNA) prior to decellularization; F. absence of any cells 5 hours after decellularization; G. presence of cellular nuclear material (DNA) prior to decellularization of hepatocellular carcinoma; H. 12 hours after decellularization of hepatocellular carcinoma < 50% cellular nuclear material is detected.

of decellularization of organs and tissues, as well as their combination, are presented in the literature. Chemical methods include the use of detergents such as SDS, sodium deoxycholate, Triton X-100 [59-61], sulfobetaine-10 (SB-10), SB-16, tri(n-butyl)phosphate (TnBP), and 3-butyl phosphate [(3-cholamidopropyl)dimethylammonio]-1-propanesulfonate (CHAPS) [62, 63]. Biological methods include enzymes, such as trypsin, deoxyribonuclease (DNase), ribonuclease (RNase) [64-66], acids, and others [67]. Mechanical methods of decellularization of organs and tissues include the use of high hydrostatic pressure (HHP), supercritical carbon dioxide, the freeze-thaw method, etc. [68-70]. Throughout recent years, decellularization methods have been developed that are based on the innate process of programmed cell death or apoptosis. Ex vivo induction of apoptosis is reported to be a promising method for tissue decellularization without the use of aggressive reagents [71, 72].

Based on our experience, we used a combination of SDS and Triton X-100 for intravital decellularization of Ehrlich's subcutaneous tumor. For an efficient of intravital decellularization, the tumor was previously subjected to the freezing/thawing procedure, which is one of

the methods of physical tissue decellularization. Due to the presence of small caliber vessels feeding the subcutaneous Ehrlich tumor, the intratumoral route was used for the administration of detergents using catheter technology. The catheters were fixated to the tumor surface with cyanoacrylate (PeriAcryl-90), which allowed to prevent chemical damage to the tissues surrounding the tumor and to minimize the percentage of detergents entering the systemic circulation. For disaggregation of tumor tissues, a warm PBS solution (37.7°C) containing 1:800 IU of collagenase A was injected, which significantly improved the perfusion of SDS and Triton X-100, and the rinsing of cancer cells from the tumor. After decellularization of the tumor, both cannulas were removed and single sutures were applied to the wound. The need for developing a protocol that limits the time of tumor decellularization in vivo was associated with the survival of animals. For example, ex vivo decellularization of a whole liver with the HCC model took > 24 hours, while the time taken to decellularize human gastric adenocarcinoma was < 12 hours, and the time to decellularize in vivo subcutaneous Ehrlich tumor (2×2 cm) was less than 5 hours. The **Figure 5** presents the assessment of the mac-

Intravital tumor decellularization

roscopic decellularization of the Ehrlich tumor depending on time. Decellularization score: good decellularization result, defined by 100% removal of both tumor cells and surrounding tissue cells, resulting in completely transparent tissue areas; Moderate decellularization result, defined by > 90% cell removal. Limited decellularization result, defined by > 50% cell removal; Poor decellularization result (1 point), defined by < 50% cell removal. Studies also showed that the tissue density of DEN-induced hepatocellular carcinoma was $0.85 \pm 0.09 \text{ cm}^3$, while the tissue density of human gastric adenocarcinoma was $0.65 \pm 0.08 \text{ cm}^3$, and the tissue density of Ehrlich's tumor was $0.54 \pm 0.07 \text{ cm}^3$.

It should be noted that, the maximum time to anaesthetize animals with ketamine, xylazine, and acepromazine is 90 minutes. Therefore, for intravital decellularization of animals with a subcutaneous Ehrlich tumor model, we used prolonged, combined anesthesia (medetomidine-midazolam-butorphanol) as recommended by the authors [73], who noted that butorphanol has an intermediate analgesic effect and can last from 6 to 8 hours in rats and from 3 to 5 hours in mice.

Administering anticancer drugs directly to the cancer parenchyma, known as intratumoral drug delivery, has both advantages and disadvantages. For example, intratumoral delivery allows the use of higher concentrations of detergents in tumor tissue, with the maximum effect of drugs on cancer cells with a minimum effect on healthy tissues. It should be noted that some tumors may have a limited blood supply or a protective microenvironment that prevents the delivery of detergents through the vessels. Internally, tumor delivery can bypass these barriers and increase the effectiveness of detergents in decellularizing any tumors. The disadvantages of intratumoral administration include the difficulty of uniform distribution of detergents throughout the tumor, which requires a significant amount of time to wash out tumor cells. Uneven distribution of detergent in the tumor can lead to untreated areas, and as a result, tumor recurrence. To prevent tumor recurrence after decellularization, hydrogels containing anti-cancer drugs can be administered. Thus, the efficacy of *in vivo* decellularization is highly dependent on tumor type and

location and must be carefully evaluated on a case-by-case basis.

In our studies, we combined the decellularization method with cryodestruction and enzymes to destroy the tumor parenchyma. Tumor cryosurgery is minimally invasive and can be used for local treatment [74]. In addition, cryodestruction can be used for various types of cancer. It also has fewer side effects compared to radiation therapy or chemotherapy. However, as our studies have shown, cryodestruction has limited effectiveness in large tumors, which manifests itself in the incomplete destruction of tumor tissue, as well as in damage to nearby healthy tissues. It is important to note that the use of enzymes to destroy the cancer parenchyma is still at an experimental stage, and further research is needed to determine their safety, efficacy, and optimal methods of administration.

Thus, we believe that intravital decellularization of tumors may open exciting new prospects in the treatment of cancerous tumors. The intravital decellularization would be more effective if detergents entered the tumor through the arteries and were extracted through the tumor veins. Unfortunately, this procedure was not possible due to the small diameter of the vessels of subcutaneous Ehrlich tumor in mice.

Conclusion

The intravital decellularization method makes it possible to remove all cellular components and DNA content from the subcutaneous Ehrlich tumor without compromising animal health. In addition, this method can destroy the extracellular matrix of the tumor, which will significantly improve the delivery of anticancer drugs to tumor cells. However, despite these results, more detailed and extensive studies are needed to develop a technique for isolated decellularization of a tumor or part of an organ with a tumor (e.g., segments of the liver) *in vivo*. It is also necessary to identify less toxic decellularization agents and develop the most effective way to deliver them to tumor cells. The intravital decellularization method can be combined with chemotherapy and immunotherapy followed by tumor resection.

Disclosure of conflict of interest

None.

Address correspondence to: Dr. Teona Paresishvili, Department of Clinical Anatomy, Tbilisi State Medical University, 33 Vazha-Pshavela Avenue, 0186 Tbilisi, Georgia. E-mail: t.paresishvili@tsmu.edu

References

- [1] Wolinsky JB, Colson YL and Grinstaff MW. Local drug delivery strategies for cancer treatment: gels, nanoparticles, polymeric films, rods, and wafers. *J Control Release* 2012; 159: 14-26.
- [2] Ma J, Wang B, Shao H, Zhang S, Chen X, Li F and Liang W. Hydrogels for localized chemotherapy of liver cancer: a possible strategy for improved and safe liver cancer treatment. *Drug Deliv* 2022; 29: 1457-1476.
- [3] Sriraman SK, Aryasomayajula B and Torchilin VP. Barriers to drug delivery in solid tumors. *Tissue Barriers* 2014; 2: e29528.
- [4] Netti PA, Berk DA, Swartz MA, Grodzinsky AJ and Jain RK. Role of extracellular matrix assembly in interstitial transport in solid tumors. *Cancer Res* 2000; 60: 2497-2503.
- [5] Teleanu RI, Chircov C, Grumezescu AM and Teleanu DM. Tumor angiogenesis and anti-angiogenic strategies for cancer treatment. *J Clin Med* 2019; 9: 84.
- [6] Spear MA, LoRusso P, Mita A and Mita M. Vascular disrupting agents (VDA) in oncology: advancing towards new therapeutic paradigms in the clinic. *Curr Drug Targets* 2011; 12: 2009-2015.
- [7] Yang T, Xiao H, Liu X, Wang Z, Zhang Q, Wei N and Guo X. Vascular normalization: a new window opened for cancer therapies. *Front Oncol* 2021; 11: 719836.
- [8] Siemann DW, Bibby MC, Dark GG, Dicker AP, Eskens FA, Horsman MR, Marmé D and Lorusso PM. Differentiation and definition of vascular-targeted therapies. *Clin Cancer Res* 2005; 11: 416-420.
- [9] Henke E, Nandigama R and Ergün S. Extracellular matrix in the tumor microenvironment and its impact on cancer therapy. *Front Mol Biosci* 2020; 6: 160.
- [10] Goodman TT, Olive PL and Pun SH. Increased nanoparticle penetration in collagenase-treated multicellular spheroids. *Int J Nanomedicine* 2007; 2: 265-274.
- [11] Fleming JM, Yeyeodu ST, McLaughlin A, Schuman D and Taylor DK. In situ drug delivery to breast cancer-associated extracellular matrix. *ACS Chem Biol* 2018; 13: 2825-2840.
- [12] Doherty GJ, Tempero M and Corrie PG. HALO-109-301: a phase III trial of PEGPH20 (with gemcitabine and nab-paclitaxel) in hyaluronic acid-high stage IV pancreatic cancer. *Future Oncol* 2018; 14: 13-22.
- [13] Tong RT, Boucher Y, Kozin SV, Winkler F, Hicklin DJ and Jain RK. Vascular normalization by vascular endothelial growth factor receptor 2 blockade induces a pressure gradient across the vasculature and improves drug penetration in tumors. *Cancer Res* 2004; 64: 3731-3736.
- [14] Winkler F, Kozin SV, Tong RT, Chae SS, Booth MF, Garkavtsev I, Xu L, Hicklin DJ, Fukumura D, di Tomaso E, Munn LL and Jain RK. Kinetics of vascular normalization by VEGFR2 blockade governs brain tumor response to radiation: role of oxygenation, angiopoietin-1, and matrix metalloproteinases. *Cancer Cell* 2004; 6: 553-563.
- [15] Davis JL, Pandalai P, Ripley RT, Langan RC, Steinberg SM, Walker M, Toomey MA, Levy E and Avital I. Regional chemotherapy in locally advanced pancreatic cancer: RECLAP trial. *Trials* 2011; 12: 129.
- [16] Murata S, Onozawa S, Mine T, Ueda T, Sugihara F, Yasui D, Kumita S, Shimizu A and Satake M. Minimizing systemic leakage of cisplatin during percutaneous isolated pancreas perfusion chemotherapy: a pilot study. *Radiol* 2015; 276: 102-109.
- [17] Lorenz M, Petrowsky H, Heinrich S, Janshon G, Staib-Sebler E, Poloczek Y, Gog C, Oremek G and Encke A. Isolated hypoxic perfusion with mitomycin C in patients with advanced pancreatic cancer. *Eur J Surg Oncol* 1998; 24: 542-547.
- [18] Burt ME, Liu D, Abolhoda A, Ross HM, Kaneda Y, Jara E, Casper ES, Ginsberg RJ and Brennan MF. Isolated lung perfusion for patients with unresectable metastases from sarcoma: a phase I trial. *Ann Thorac Surg* 2000; 69: 1542-1549.
- [19] Davies EJ, Reijers SJM, Van Akkooi ACJ, Van Houdt WJ and Hayes AJ. Isolated limb perfusion for locally advanced melanoma in the immunotherapy era. *Eur J Surg Oncol* 2022; 48: 1288-1292.
- [20] Van Veenendaal LM, Madu MF, Tesselaar MET, Verhoef C, Grünhagen DJ and Van Akkooi ACJ. Efficacy of isolated limb perfusion (ILP) in patients with Merkel cell carcinoma (MCC): a multicenter experience. *Eur J Surg Oncol* 2017; 43: 2157-2162.
- [21] Hoekstra HJ, Veerman K and Van Ginkel RJ. Isolated limb perfusion for in-transit melanoma metastases: melphalan or TNF-melphalan perfusion? *J Surg Oncol* 2014; 109: 338-347.
- [22] Sevilla-Ortega L, Ferrándiz-Pulido L, Palazón-Carrión N, Álamo De La Gala MDC, De Toro-Salas R, Garnacho-Montero J, Marcos-Rodríguez JA, Agudo Martínez A, Araji-Tiliani O, Calvo-Morón MC, Barquero-Aroca JM, Fernández-López AR, Jaime-Borrego JM, Santos-Jimé-

- nez JC, Moreno-Ramírez D and De La Cruz-Merino L. Role of isolated limb perfusion in the era of targeted therapies and immunotherapy in melanoma. A systematic review of the literature. *Cancers (Basel)* 2021; 13: 5485.
- [23] Lang H, Nadalin S, Thyen A, Moreno L, Shehata SR, Schüttler W and Oldhafer KJ. A porcine model for investigation of hyperthermic isolated liver perfusion. *J Invest Surg* 1998; 11: 401-408.
- [24] Zhang J, Li M, Chen Z, OuYang J and Ling Z. Efficacy of bladder intravesical chemotherapy with three drugs for preventing non-muscle-invasive bladder cancer recurrence. *J Healthc Eng* 2021; 2021: 2360717.
- [25] Raz E, Cavalcanti DD, Sen C, Nossek E, Potts M, Peschillo S, Lotan E, Narayan V, Ali A, Sharashidze V, Nelson PK and Shapiro M. Tumor embolization through meningoypophyseal and inferolateral trunks is safe and effective. *AJNR Am J Neuroradiol* 2022; 43: 1142-1147.
- [26] Akimoto T, Ohtake M, Miyake S, Suzuki R, Iida Y, Shimohigoshi W, Higashijima T, Nakamura T, Shimizu N, Kawasaki T, Sakata K and Yamamoto T. Preoperative tumor embolization prolongs time to recurrence of meningiomas: a retrospective propensity-matched analysis. *J Neurointerv Surg* 2023; 15: 814-820.
- [27] Ou D, Chen C, Jiang T and Xu D. Research review of thermal ablation in the treatment of papillary thyroid carcinoma. *Front Oncol* 2022; 12: 859396.
- [28] Van Den Hoven AF, Lam MG, Jernigan S, Van Den Bosch MA and Buckner GD. Innovation in catheter design for intra-arterial liver cancer treatments results in favorable particle-fluid dynamics. *J Exp Clin Cancer Res* 2015; 34: 74.
- [29] Yin L and Li J. Central venous catheter insertion in colorectal cancer patients, PICC or PC? *Cancer Manag Res* 2020; 12: 5813-5818.
- [30] Wu O, McCartney E, Heggie R, Germeni E, Paul J, Soulis E, Dillon S, Ryan C, Sim M, Dixon-Hughes J, Agarwal R, Bodenham A, Menne T, Jones B and Moss J. Venous access devices for the delivery of long-term chemotherapy: the CAVA three-arm RCT. *Health Technol Assess* 2021; 25: 1-126.
- [31] Patel GS, Jain K, Kumar R, Strickland AH, Pellegrini L, Slavotinek J, Eaton M, McLeay W, Price T, Ly M, Ullah S, Koczwara B, Kichenadasse G and Karapetis CS. Comparison of peripherally inserted central venous catheters (PICC) versus subcutaneously implanted port-chamber catheters by complication and cost for patients receiving chemotherapy for non-haematological malignancies. *Support Care Cancer* 2014; 22: 121-128.
- [32] Facy O, Doussot A, Zinzindohoué F, Holl S, Rat P and Ortega Deballon P. Isolated hepatic perfusion: Principles and results. *J Visc Surg* 2014; 151 Suppl 1: S25-32.
- [33] Wang A, Kuriata O, Xu F, Nietzsche S, Gremse F, Dirsch O, Settmacher U and Dahmen U. A survival model of *in vivo* partial liver lobe decellularization towards *in vivo* liver engineering. *Tissue Eng Part C Methods* 2020; 26: 402-417.
- [34] Yaldiz B, Saglam-Metiner P and Yesil-Celiktas O. Decellularised extracellular matrix-based biomaterials for repair and regeneration of central nervous system. *Expert Rev Mol Med* 2021; 23: e25.
- [35] Tiemann TT, Padma AM, Sehic E, Bäckdahl H, Oltean M, Song MJ, Brännström M and Hellström M. Towards uterus tissue engineering: a comparative study of sheep uterus decellularisation. *Mol Hum Reprod* 2020; 26: 167-178.
- [36] Akbarzadeh A, Kianmanesh M, Fendereski K, Ebadi M, Daryabari SS, Masoomi A, Ghazisaeedi F, Seyyed Hossein Beigi R, Sheikh R and Kajbafzadeh AM. Decellularised whole ovine testis as a potential bio-scaffold for tissue engineering. *Reprod Fertil Dev* 2019; 31: 1665-1673.
- [37] O'Connor Mooney R, Davis NF, Hoey D, Hogan L, McGloughlin TM and Walsh MT. On the automatic decellularisation of porcine aortae: a repeatability study using a non-enzymatic approach. *Cells Tissues Organs* 2016; 201: 299-318.
- [38] Grey JFE, Campbell-Ritchie A, Everitt NM, Fezovich AJ and Wheatley SP. The use of decellularised animal tissue to study disseminating cancer cells. *J Cell Sci* 2018; 132: jcs219907.
- [39] Wang C, Zhao Q, Zheng X, Li S, Chen J, Zhao H, Chen F, Cui L and Li W. Decellularized brain extracellular matrix slice glioblastoma culture model recapitulates the interaction between cells and the extracellular matrix without a nutrient-oxygen gradient interference. *Acta Biomater* 2023; 158: 132-150.
- [40] Iazzolino G, Mendibil U, Arnaiz B, Ruiz-de-Angulo A, Azkargorta M, Uribe KB, Khatami N, Elortza F, Olalde B, Gomez-Vallejo V, Llop J and Abarrategi A. Decellularization of xenografted tumors provides cell-specific *in vitro* 3D environment. *Front Oncol* 2022; 12: 956940.
- [41] VandenHeuvel SN, Farris HA, Noltensmeyer DA, Roy S, Donehoo DA, Kopetz S, Haricharan S, Walsh AJ and Raghavan S. Decellularized organ biomatrices facilitate quantifiable *in vitro* 3D cancer metastasis models. *Soft Matter* 2022; 18: 5791-5806.
- [42] Kakabadze Z, Kakabadze A, Chakhunashvili D, Karalashvili L, Berishvili E, Sharma Y and Gupta S. Decellularized human placenta supports hepatic tissue and allows rescue in acute liver failure. *Hepatology* 2018; 67: 1956-1969.

- [43] Kurma K, Manches O, Chuffart F, Sturm N, Gharzeddine K, Zhang J, Mercey-Ressejac M, Rousseaux S, Millet A, Lerat H, Marche PN, Macek Jilkova Z and Decaens T. DEN-induced rat model reproduces key features of human hepatocellular carcinoma. *Cancers (Basel)* 2021; 13: 4981.
- [44] Jacob G, Li AK and Hobbs KE. A comparison of cryodestruction with excision or infarction of an implanted tumor in rat liver. *Cryobiology* 1984; 21: 148-156.
- [45] Tashiro M, Hosokawa Y, Amao H and Tohei A. Duration of thermal support for preventing hypothermia induced by anesthesia with medetomidine-midazolam-butorphanol in mice. *J Vet Med Sci* 2020; 82: 1757-1762.
- [46] Felgendreff P, Schindler C, Mussbach F, Xie C, Gremse F, Settmacher U and Dahmen U. Identification of tissue sections from decellularized liver scaffolds for repopulation experiments. *Heliyon* 2021; 7: e06129.
- [47] Abdeljalil SM, Wahdan SA, Elghazaly H and Tolba MF. Insights into the therapeutic outcomes of trimetazidine/doxorubicin combination in Ehrlich solid-phase carcinoma mouse tumor model. *Life Sci* 2023; 328: 121874.
- [48] Alghamdi MA, Khalifah TA, Alhawati HS, Ruzayq M, Alrakaf A, Khodier A and Al-Gayyar MM. Antitumor activity of ferulic acid against ehrlich solid carcinoma in rats via affecting hypoxia, oxidative stress and cell proliferation. *Cureus* 2023; 17; 15: e41985.
- [49] Kučan D, Oršolić N, Odeh D, Ramić S, Jakopović B, Knežević J and Jazvinščak Jembrek M. The role of hyperthermia in potentiation of anti-angiogenic effect of cisplatin and resveratrol in mice bearing solid form of ehrlich ascites tumour. *Int J Mol Sci* 2023; 24: 11073.
- [50] Aldubayan MA, Elgharabawy RM, Ahmed AS and Tousson E. Antineoplastic activity and curative role of avenanthramides against the growth of ehrlich solid tumors in mice. *Oxid Med Cell Longev* 2019; 2019: 5162687.
- [51] Kodama M, Kodama T and Nishi Y. Differential surface structures of invasive and non-invasive Ehrlich ascites tumor cell lines with special reference to the effect of hydrocortisone treatment. *Anticancer Res* 1992; 12: 1217-21.
- [52] Mishra S, Tamta AK, Sarikhani M, Desingu PA, Kizkekra SM, Pandit AS, Kumar S, Khan D, Raghavan SC and Sundaresan NR. Subcutaneous Ehrlich Ascites Carcinoma mice model for studying cancer-induced cardiomyopathy. *Sci Rep* 2018; 8: 5599.
- [53] Mondal B and Saha S. Inhibition of subcutaneous growth of Ehrlich ascites carcinoma (EAC) tumor by post-immunization with EAC-cell gangliosides and its anti-idiotypic antibody in relation to tumor angiogenesis, apoptosis, cell cycle and infiltration of CD4+, CD8+ lymphocytes, NK cells, suppressor cells and APC-cells in tumor. *Indian J Exp Biol* 2011; 49: 574-84.
- [54] Castelló CM, Miguel MP, Silveira-Lacerda EP, Bakuzis AF and Borges NC. B-mode and doppler ultrasonography in a murine model of ehrlich solid carcinoma with different growth patterns. *Front Oncol* 2020; 10: 560413.
- [55] Kakabadze Z, Karalashvili L, Chakhunashvili D, Havlioglu N, Janelidze M, Kakabadze A, Sharma Y and Gupta S. Decellularized bovine placentome for portacavally-interposed heterotopic liver transplantation in rats. *Mater Sci Eng C Mater Biol Appl* 2019; 97: 293-301.
- [56] Kakabadze A, Mardaleishvili K, Loladze G, Karalashvili L, Chutkerashvili G, Chakhunashvili D and Kakabadze Z. Reconstruction of mandibular defects with autogenous bone and decellularized bovine bone grafts with freeze-dried bone marrow stem cell paracrine factors. *Oncol Lett* 2017; 13: 1811-1818.
- [57] Kakabadze Z, Chakhunashvili D, Gogilashvili K, Ediberidze K, Chakhunashvili K, Kalandarishvili K and Karalashvili L. Bone marrow stem cell and decellularized human amniotic membrane for the treatment of nonhealing wound after radiation therapy. *Exp Clin Transplant* 2019; 17 Suppl 1: 92-98.
- [58] Chakhunashvili K, Kiladze M, G Chakhunashvili D, Karalashvili L and Kakabadze Z. A three-dimensional scaffold from decellularized human umbilical artery for bile duct reconstruction. *Ann Ital Chir* 2019; 90: 165-173.
- [59] White LJ, Taylor AJ, Faulk DM, Keane TJ, Saldin LT, Reing JE, Swinehart IT, Turner NJ, Ratner BD and Badylak SF. The impact of detergents on the tissue decellularization process: a ToF-SIMS study. *Acta Biomater* 2017; 50: 207-219.
- [60] Cheng J, Li J, Cai Z, Xing Y, Wang C, Guo L and Gu Y. Decellularization of porcine carotid arteries using low-concentration sodium dodecyl sulfate. *Int J Artif Organs* 2021; 44: 497-508.
- [61] Narciso M, Uldemolins A, Júnior C, Otero J, Navajas D, Farré R, Gavara N and Almendros I. Novel decellularization method for tissue slices. *Front Bioeng Biotechnol* 2022; 10: 832178.
- [62] O'Neill JD, Anfang R, Anandappa A, Costa J, Javidfar J, Wobma HM, Singh G, Freytes DO, Bacchetta MD, Sonett JR and Vunjak-Novakovic G. Decellularization of human and porcine lung tissues for pulmonary tissue engineering. *Ann Thorac Surg* 2013; 96: 1046-1055; discussion 1055-1056.
- [63] Tebyanian H, Karami A, Motavallian E, Aslani J, Samadikuchaksaraei A, Arjmand B and Nourani MR. A comparative study of rat lung decellularization by chemical detergents for lung tissue engineering. *Open Access Maced J Med Sci* 2017; 5: 859-865.

Intravital tumor decellularization

- [64] Crapo PM, Gilbert TW and Badylak SF. An overview of tissue and whole organ decellularization processes. *Biomaterials* 2011; 32: 3233-3243.
- [65] Moffat D, Ye K and Jin S. Decellularization for the retention of tissue niches. *J Tissue Eng* 2022; 13: 204173142211011.
- [66] Giraldo-Gomez DM, Leon-Mancilla B, Del Prado-Audelo ML, Sotres-Vega A, Villalba-Caloca J, Garciadiego-Cazares D and Piña-Barba MC. Trypsin as enhancement in cyclical tracheal decellularization: morphological and biophysical characterization. *Mater Sci Eng C Mater Biol Appl* 2016; 59: 930-937.
- [67] Yamanaka H, Morimoto N and Yamaoka T. Decellularization of submillimeter-diameter vascular scaffolds using peracetic acid. *J Artif Organs* 2020; 23: 156-162.
- [68] Zemmyo D, Yamamoto M and Miyata S. Fundamental study of decellularization method using cyclic application of high hydrostatic pressure. *Micromachines (Basel)* 2020; 11: 1008.
- [69] Guler S, Aslan B, Hosseinian P and Aydin HM. Supercritical carbon dioxide-assisted decellularization of aorta and cornea. *Tissue Eng Part C Methods* 2017; 23: 540-547.
- [70] Burk J, Erbe I, Berner D, Kacza J, Kasper C, Pfeiffer B, Winter K and Brehm W. Freeze-Thaw cycles enhance decellularization of large tendons. *Tissue Eng Part C Methods* 2014; 20: 276-284.
- [71] Song YH, Maynes MA, Hlavac N, Visosevic D, Daramola KO, Porvasnik SL and Schmidt CE. Development of novel apoptosis-assisted lung tissue decellularization methods. *Biomater Sci* 2021; 9: 3485-3498.
- [72] Cornelison RC, Wellman SM, Park JH, Porvasnik SL, Song YH, Wachs RA and Schmidt CE. Development of an apoptosis-assisted decellularization method for maximal preservation of nerve tissue structure. *Acta Biomater* 2018; 77: 116-126.
- [73] Gades NM, Danneman PJ, Wixson SK and Tolley EA. The magnitude and duration of the analgesic effect of morphine, butorphanol, and buprenorphine in rats and mice. *Contemp Top Lab Anim Sci* 2000; 39: 8-13.
- [74] Yiu WK, Basco MT, Aruny JE, Cheng SW and Sumpio BE. Cryosurgery: a review. *Int J Angiol* 2007; 16: 1-6.